Conformational Differences in *Mycobacterium tuberculosis* Catalase-Peroxidase KatG and Its S315T Mutant Revealed by Resonance Raman Spectroscopy†

Sofia Kapetanaki,‡ Salem Chouchane,§ Stefania Girotto,§ Shengwei Yu,§ Richard S. Magliozzo,§ and Johannes P. M. Schelvis*,‡

Department of Chemistry, New York University, 31 Washington Place, Room 1001, New York, New York 10003, and Department of Chemistry, Brooklyn College and the Graduate Center of the City University of New York, 2900 Bedford Avenue, Brooklyn, New York 11210-2889

Received October 11, 2002; Revised Manuscript Received January 14, 2003

ABSTRACT: KatG from *Mycobacterium tuberculosis* is a heme-containing catalase-peroxidase, which belongs to the class I peroxidases and is important for activation of the prodrug isoniazid (INH), a front-line antituberculosis drug. In many clinical isolates, resistance to INH has been linked to mutations on the *kat*G gene, and the most prevalent mutation, S315T, suggests that modification of the heme pocket has occurred. Electronic absorption and resonance Raman spectra of ferric wild-type (WT) KatG and its INH-resistant mutant KatG(S315T) at different pH values and their complexes with INH and benzohydroxamic acid (BHA) are reported. At neutral pH, a quantum mechanically mixed spin state (QS) is revealed, which coexists with five-coordinate and six-coordinate high-spin hemes in WT KatG. The QS heme is the major species in KatG(S315T). Addition of either INH or BHA to KatG induces only minor changes in the resonance Raman spectra, indicating that both compounds do not directly interact with the heme iron. New vibrational modes are observed at 430, 473, and 521 cm^{-1}, and these modes are indicative of a change in conformation in the KatG heme pocket. The intensity of these modes and the relative population of the QS heme are stable in KatG(S315T) but not in the WT enzyme. This indicates that there are differences in heme pocket stability between WT KatG and KatG(S315T). We will discuss the stabilization of the QS heme and propose a model for the inhibition of INH oxidation by KatG(S315T).

Mycobacterium tuberculosis infection is the second leading cause of death worldwide among known infectious diseases (*1*). Isoniazid (INH)[1] has been the cornerstone in tuberculosis chemotherapy for almost half a century since its discovery as a potent antituberculosis drug in 1952 (*2*). Although its mechanism of action is not fully understood, two enzymes involved in mycolic acid synthesis, InhA (NADH-dependent enoyl-ACP reductase) and kasA (β-ketoacyl-ACP synthase), are believed to be inhibited by a metabolite of INH (*3*−*5*), which is generated by functional catalase-peroxidase *M. tuberculosis* KatG (*6*−*11*). Immediately after its introduction, resistance to INH was observed, and in the majority of clinical isolates, mutations of the *kat*G gene encoding catalase−peroxidase were linked to INH resistance (*11*). The most frequently encountered mutation is the S315T substitution, which has been found in >50% of resistant isolates (*12*−*20*). On the basis of sequence homologies with cytochrome *c* peroxidase (CCP) and ascorbate peroxidases (APXs), the bacterial catalase-peroxidases have been classified as class I peroxidases (*21*). Peroxidases belonging to the superfamily of plant peroxidases are generally divided in three classes according to their origin. Class I includes the intracellular peroxidases of prokaryotic origin, class II constitutes the secretory fungal peroxidases, and class III contains the classical secretory plant peroxidases (*21*). KatGs are homomultimeric proteins with monomers approximately double in size compared to those of CCP or APXs, due to gene duplication (*22*). Sequence alignment of catalase−peroxidases (*23*) suggests that they also have conserved the amino acid triad Arg/Trp/His in the distal heme pocket and the triad His/Trp/Asp in the proximal heme pocket similar to class I peroxidases. Despite the striking sequence homologies, there are significant differences in catalytic activity and substrate specificity between KatGs and class I peroxidases. KatGs exhibit both catalase activity comparable with catalases and typical peroxidase activity with broad specificity (*6*).

The *M. tuberculosis* catalase-peroxidase (KatG) is a bifunctional enzyme that exists as a homodimer of 80 kDa subunits, both of which contain one heme iron (*24*, *25*). Besides the catalase-peroxidase activity, Mn^{2+}-dependent peroxidase, cytochrome P450-like oxygenase, and peroxynitritase activities have also been reported (*6*, *11*, *24*−*28*).

† This work was supported by start-up funds from New York University (J.P.M.S.) and National Institutes of Health Grant AI-43582 (National Institute of Allergy and Infectious Diseases) (R.S.M.).

* To whom correspondence should be addressed: tel, (212) 998-3597; fax, (212) 260-0795; e-mail, hans.schelvis@nyu.edu.

‡ New York University.

§ Brooklyn College and the Graduate Center of the City University of New York.

[1] Abbreviations: *M. tuberculosis*, *Mycobacterium tuberculosis*; WT, wild type; 6-c, six coordinate; 5-c, five coordinate; LS, low spin; HS, high spin; QS, quantum mechanically mixed spin; EPR, electron paramagnetic resonance; INH, isoniazid (isonicotinic acid hydrazide); CCP, cytochrome *c* peroxidases; APX, ascorbate peroxidases; CIP, *Coprinus cinereus* peroxidases; HRPA2, horseradish peroxidase isozyme A2; TcAPXII, tea cationic ascorbate peroxidase isoenzyme II; *Hm*CP, *Haloarcula marismortui* catalase-peroxidase.

10.1021/bi026992y CCC: $25.00
Published on Web 03/14/2003

Although crystals have been grown of several catalase-peroxidases, no crystal structure of a KatG was available until very recently when the crystal structure of a catalase-peroxidase from *Haloarcula marismortui* was determined at 2.0 Å resolution (*29*−*31*). On the basis of sequence alignment with *Saccharomyces cerevisiae* CCP and *Hm*CP KatG, the *M. tuberculosis* KatG amino acid residue Ser315 (analogous to CCP Ser185 and *Hm*CP Ser305) hydrogen bonds to a heme propionate, which suggests that modification of the heme pocket gives rise to INH resistance in KatG-(S315T). Structural information about the KatG active site has mainly been obtained by spectroscopic techniques and comparison to the crystal structures of CCP and APX based on sequence homology (*32*−*41*). Recent spectroscopic data have revealed a histidine residue with imidazolate character as the proximal heme ligand in *M. tuberculosis* KatG (*36*). UV−vis and resonance Raman data suggest that the distal heme environment of ferric and ferrous KatG(S315T) is altered relative to wild-type (WT) KatG as demonstrated by a greater population of six-coordinate, low-spin (6-c LS) heme in KatG(S315T) (*36*, *37*). In these studies, some 6-c LS was reported for WT KatG (*36*), while in a similar study only a trace amount of a 6-c LS ferric heme could be detected (*35*). In the latter case, the majority of the heme iron species is five-coordinate, high spin (5-c HS), but heterogeneity in heme spin state increases as the isolated enzyme ages during storage (*41*, *35*). A recent report on KatG from the cyanobacterium *Synechocystis* demonstrated the presence of 5-c HS, 6-c HS, and 6-c LS heme species, underscoring the heme spin state heterogeneity in KatGs (*42*). Resonance Raman studies on the CO complexes of WT KatG and KatG(S315T) also indicated differences in the heme environment of these two enzymes, though INH did not disturb the heme environment of the heme−CO complex (*37*).

The affinity of INH to WT KatG has been reported to be cooperative with a dissociation constant of 2.2 μM, while INH concentrations as high as 1 mM do not induce a change in the absorption spectrum of KatG(S315T) (*38*). Even though there are large differences in affinity, it has been observed that KatG(S315T) oxidizes INH with a rate equivalent to that of the WT enzyme after addition of alkyl peroxides (*39*; R. S. Magliozzo, unpublished results). On the basis of NMR ^{15}N relaxation measurements, the distance between the heme iron and an INH amide nitrogen has been estimated to be approximately 4 Å for both WT KatG and KatG(S315T) (*38*, *40*). EPR and resonance Raman data indicate that addition of INH to the WT enzyme and the mutant induces a small change in heme coordination state from 6-c HS to 5-c HS, in agreement with the 2 nm blue shift of the Soret absorption band of WT KatG (*36*, *38*).

In this work, we use electronic absorption and resonance Raman spectroscopies to investigate the heme pocket properties of our ferric WT KatG and KatG(S315T) preparations and their complexes with INH and benzohydroxamic acid (BHA) to obtain a better understanding of the effect of the S315T mutation and INH binding on the heme and its protein environment. Our study reveals the existence of a 5-c quantum spin (QS) heme that coexists with 5-c and 6-c HS heme species. To the best of our knowledge, this is the first time that such a species has been observed in a class I peroxidase. Furthermore, we observe enhancement of new vibrational modes of the heme cofactor at 430, 473, and 521 cm^{-1} after addition of INH to WT KatG, in the S315T mutant, and at alkaline pH. The QS heme and the enhancement of the low-frequency vibrations were not observed in earlier resonance Raman investigations of KatGs (*37*, *42*). The enhancement of the low-frequency vibrations suggests that conformational changes have occurred in the KatG heme pocket. We investigate the origin of the QS heme and the enhancement of these vibrations by comparison of KatG with BHA-bound horseradish peroxidase isozyme C (HRP-C) (*43*) and the recent crystal structure of *Hm*CP KatG (*31*). Finally, we discuss a model for the inhibition of INH oxidation in KatG(S315T).

MATERIALS AND METHODS

Materials. The plasmid pKAT II (a gift from Stewart Cole, Institut Pasteur, Paris) (*24*) was used as an overexpression vector for KatG and as the source for the *kat*G gene which was cloned into pKS II$^+$ to generate pSY15 used for mutagenesis. *Escherichia coli* strain DH5α was used as a host for the plasmids and cloning procedures; BMH71-18 *mut*S was used in the mutagenesis step. Strain UM262 (*recA katG::*Tn*10 pro leu rpsL hsdMhsdR endl lacY*) (*44*) was used for KatG and KatG(S315T) overexpression. The site-directed mutagenesis kit was from Clontech (Palo Alto, CA). $H_2{}^{18}O$ (95% enrichment) was purchased from Medical Isotopes, Inc. All other reagents were from Sigma-Aldrich.

Site-Directed Mutagenesis of the M. tuberculosis katG Gene. Mutagenesis was performed using the Transformer site-directed mutagenesis kit from Clontech (Palo Alto, CA). The 1.0 kb *Cla*I−*Xho*I fragment of the *kat*G gene was subcloned into the pKS II$^+$ vector in a two-step cloning process to generate pSY15, in which site-directed mutagenesis was performed. The mutagenesis primer was CGATCACCA**C**CGGCATCGAGGT (S315T); the selection primer was CTGTGACTGGTGAG**AT**CTCAACCAAGTC; a unique restriction site (*Sca*I) was replaced by a new unique restriction site (*Bgl*II) (letters in boldface type indicate base(s) changed during mutagenesis; the underlined portion of the sequence represents the restriction enzyme site after conversion). Sequence confirmation was done on double-stranded plasmid DNA by the Sanger method (*45*) through Gene Link, Inc. (Hawthorne, NY), to confirm the desired nucleotide substitution. The confirmed mutated *kat*G insert was excised from the pKS II$^+$ vector using restriction enzymes *Nhe*I and *Xho*I. This *Nhe*I−*Xho*I fragment containing the S315T mutation was ligated to the pKAT vector to replace the corresponding wild-type fragment and generate pSY31.

Isolation and Purification of M. tuberculosis Catalase-Peroxidase. The catalase-peroxidase used in this study was isolated and purified from an overexpression system in *E. coli* strain UM262 (KatG minus) expressing the *M. tuberculosis kat*G gene. The bacteria were grown in the presence of the heme biosynthetic precursor, δ-aminolevulinic acid. The enzyme was purified by FPLC according to a published procedure with minor modification (*26*). The purified enzyme was in 20 mM potassium phosphate buffer at pH 7.2. All of the samples used in this study were 2 weeks old to avoid changes in heme spin state distribution due to aging of the protein unless stated otherwise. These changes associated with purification procedures and storage are well documented in a recent publication (*41*). For the pH studies, KatG samples

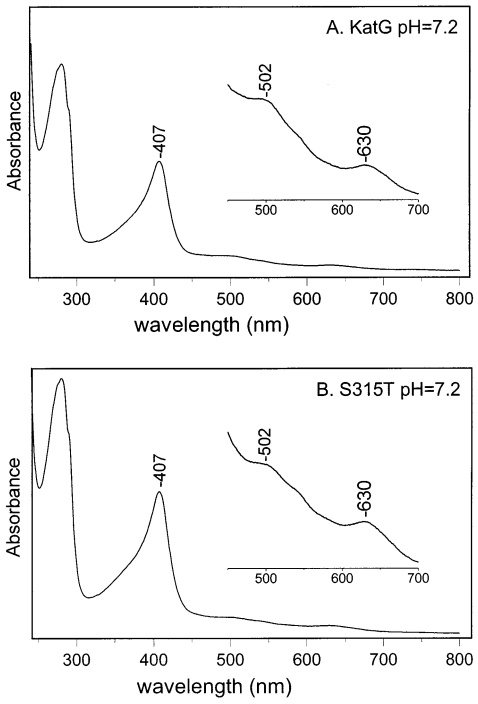

FIGURE 1: UV−vis spectra of wild-type KatG (A) and KatG-(S315T) (B) at pH = 7.2.

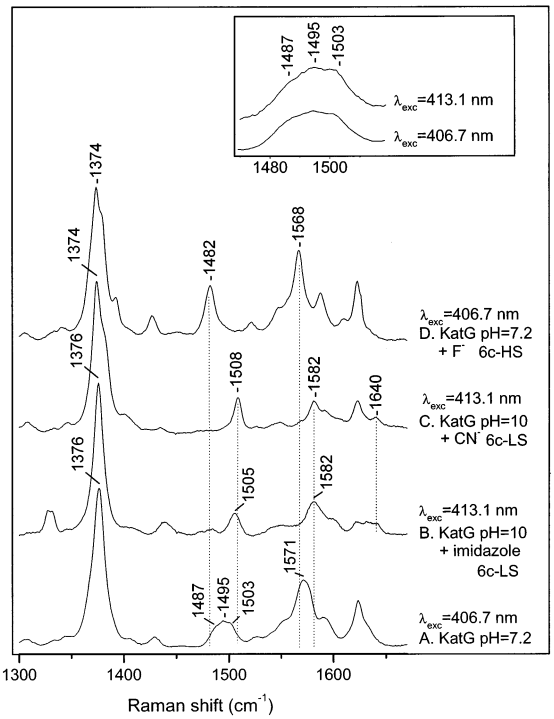

FIGURE 2: High-frequency resonance Raman spectra of ferric wild-type KatG obtained with 406.7 nm excitation at pH = 7.2 (A), its complex with imidazole at pH = 10 with 413.1 nm excitation (B), its complex with cyanide at pH = 10 with 413.1 nm excitation (C), and its complex with fluoride at pH = 7.2 with 406.7 nm excitation (D). Inset: ν_3 region of wild-type KatG at pH = 7.2 with 406.7 and 413.1 nm excitation.

were transferred to 20 mM citrate buffer at pH 5 or 20 mM borate buffer at pH 10. The D_2O samples were prepared by diluting the protein in the corresponding D_2O buffer solutions and concentrating to yield 90−95% enrichment. KatG was dissolved in H_2O, D_2O, and $H_2{}^{18}O$ buffered solutions and left to exchange for 1 day.

Electronic Absorption and Resonance Raman Spectroscopy. Electronic absorption spectra were recorded at room temperature with a UV−vis spectrophotometer (Lambda P40 Perkin-Elmer). The resonance Raman spectra were obtained using a single spectrograph (TriAx 550, JY/Horiba) and a N_2(l)-cooled CCD detector (Spectrum One, JY/Horiba) with a UV-enhanced 2048 × 512 pixel chip (EEV). The Rayleigh scattering was removed by using a 413.1 nm holographic notch filter (Kaiser Optical). The samples were excited with either the 406.7 or the 413.1 nm line from a Kr^+ laser (Coherent, I-302). The samples were placed in a spinning cell under an N_2 atmosphere and kept at 6 ± 2 °C during the experiments. Sample concentration was 40 μM, and the laser power incident on the sample was 10 mW. The KatG−INH, KatG−BHA, and KatG(S315T)−INH complexes were prepared by addition of 10, 15, and 500 equiv of the corresponding compound, respectively. The resonance Raman spectra were corrected for a background by subtracting a polynomial function. The vibrational modes were labeled and assigned following the literature unless indicated differently (*46*−*48*). Toluene was used to calibrate the resonance Raman spectra. To determine relative peak intensities and positions, a curve-fitting program was used to simulate experimental spectra using Lorentzian line shapes. A bandwidth of 13.5 cm^{-1} was used for the simulation of the ν_3 region following the literature (*49*).

RESULTS

Electronic absorption spectra of KatG and KatG(S315T) are shown in Figure 1. The Soret band appears at 407 nm for both proteins, whereas a broad porphyrin-to-metal charge transfer band (CT1) is observed at 630 nm. The CT1 band, which is observed only in ferric high-spin heme proteins, ranges from 600 to 637 nm for 6-c hemes and ranges from 640 to 652 nm for 5-c hemes with an imidazole as the proximal ligand. The absorption spectra in Figure 1 are therefore indicative of high-spin heme. No low-spin heme absorption bands are observed between 565 and 580 nm for either the wild type or the mutant at the three pHs studied (*39*). Furthermore, the extinction coefficients for the α and β bands of 6-c LS peroxidase complexes are nearly 5-fold larger than those at similar wavelengths for HS ferric peroxidases (*50*). Therefore, no significant amount of low-spin heme is present in our samples.

Figure 2 shows the high-frequency resonance Raman spectra of KatG and of its 6-c LS complexes with imidazole and cyanide and its 6-c HS complex with fluoride at 280 K and at the indicated pH and excitation wavelength. The heme vibrations above 1300 cm^{-1} have been shown to be sensitive markers of the oxidation state, the coordination number, and the spin state of the heme as well as of the C═C vinyl stretching vibrations (*51*). The ν_4 band, which is known as the oxidation state marker, is observed at 1376 cm^{-1} for WT KatG (A), a frequency typical of an Fe(III) heme. The resonance Raman spectrum of WT KatG shows a complicated ν_3 region. Curve fitting of the ν_3 band reveals three almost equally populated components at 1487, 1495, and 1503 cm^{-1} (Table 1; fits are shown in Supporting Information). The ν_3 mode at 1495 cm^{-1} is typical of a 5-c HS ferric heme. The vibration at 1487 cm^{-1} is attributed to a 6-c HS ferric heme, and it has a slightly higher frequency than in

Table 1: Contribution (%) of the Three Heme Spin States

	ν_3 = 1487 cm^{-1}, 6-c HS heme (%)	ν_3 = 1495 cm^{-1}, 5-c HS heme (%)	ν_3 = 1503 cm^{-1}, QS heme (%)
KatG WT			
pH = 5	34 ± 1	37 ± 2	29 ± 1
pH = 5 + INH	25	40	35
pH = 7.2	33 ± 1	35 ± 4	32 ± 3
pH = 7.2 + INH	27	36	37
pH = 7.2 + BHA	28	39	33
pH = 10	22 ± 3	37 ± 1	40 ± 3
pH = 10 + INH	23	38	39
KatG(S315T)			
pH = 5	43	36	21
pH = 7.2	13	38	49
pH = 7.2 + INH	11	40	50
pH = 10	10	39	51
fresh KatG WT	8	38	54
fresh KatG(S315T)		42	58

the 6-c HS fluoride complex (D). The ν_3 vibration with a frequency of 1503 cm^{-1} could be interpreted as a 6-c LS heme species, but three observations argue against such an assignment. First, as mentioned above, the absorption spectrum of WT KatG shows no bands due to a LS heme. Second, low-temperature EPR spectroscopy indicates that the amount of 6-c LS heme in our preparation is small (<10%) in WT KatG (*41*). Third, excitation of WT KatG at 413.1 nm to enhance a potential low-spin heme does not result in an increase of the intensity of the 1503 cm^{-1} vibration (Figure 2, inset). This is in contrast with an earlier study on *M. tuberculosis* KatG where small and large increases in the intensity of the 1503 cm^{-1} band were observed in WT KatG and KatG(S315T), respectively, when a LS heme was excited at 413.1 nm (*36*). Moreover, addition of imidazole and cyanide to KatG to form a low-spin heme results in ν_3 vibrations with higher frequencies at 1505 and 1508 cm^{-1}, respectively. An alternative assignment of the ν_3 band at 1503 cm^{-1} is to a quantum mechanically mixed spin (QS) species, which results from the admixture of high ($S = {}^5/_2$) and intermediate ($S = {}^3/_2$) spin states (*52*, *53*) and has been reported for *Chromatium* ferricytochrome *c* (*52*, *54*) and several class III peroxidases (*48*, *55*−*59*; Table 2), but its observation in a class I peroxidase is new.

Figure 3 shows the high-frequency resonance Raman spectra of KatG excited at 406.7 nm at acidic, neutral, and alkaline pH at 280 K. The ν_4 band is observed at 1376 cm^{-1}, for all three pH values, but the coordination and spin states of the heme are affected by variation of pH (Table 1; fits are shown in Supporting Information). The three heme species are observed at acidic and neutral pH with similar

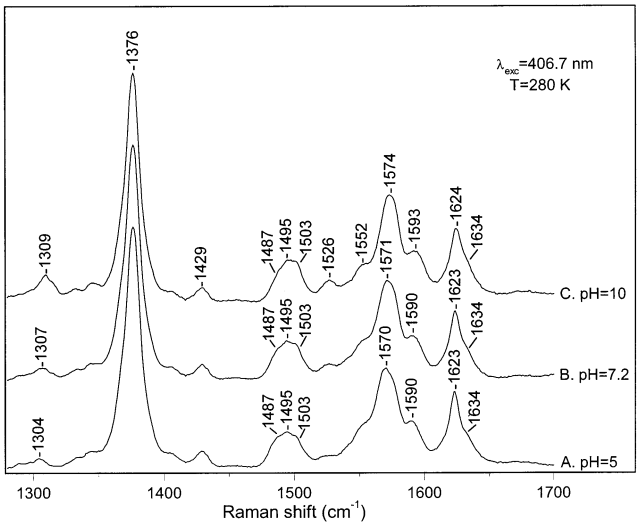

FIGURE 3: High-frequency resonance Raman spectra of ferric wild-type KatG obtained with 406.7 nm excitation at pH = 5 (A), pH = 7.2 (B), and pH = 10 (C).

relative intensities, and the 5-c HS species dominates slightly. At pH 10, the QS species, with ν_3 at 1503 cm^{-1}, gains intensity at the expense of the 6-c HS and becomes the major spin species. At pH 5, the ν_2 region shows a band centered at 1570 cm^{-1} with two shoulders at 1590 and 1552 cm^{-1}. As the pH is raised from 5 to 10, the ν_2 mode at 1570 cm^{-1} and the ν_{19} mode at 1590 cm^{-1} upshift, the ν_{11} mode at 1552 cm^{-1} band becomes more resolved, and the ν_{38} mode at 1526 cm^{-1} gains intensity. The large overlap of bands in the ν_2 region and the presence of three heme species complicate a straightforward assignment of the above-mentioned vibrations. However, the shift patterns observed with increasing pH are in agreement with a change from 6-c HS ($\nu_2 = 1568$ cm^{-1}) to 5-c QS ($\nu_2 \approx 1582$ cm^{-1}) (*48*, *60*). The resonance Raman spectral region between 1600 and 1650 cm^{-1} is also complex. In this region, the vinyl stretching vibrations and the porphyrin ν_{10} modes are expected. The band at 1623 cm^{-1} and a shoulder around 1634 cm^{-1} are tentatively attributed to the vinyl stretching vibrations (*60*). It has been proposed that when the protein matrix exerts no constraints on the vinyl groups, two distinct vinyl stretching modes should be observed in their resonance Raman spectrum: one band, around 1620 cm^{-1}, assigned to a nearly in-plane vinyl group and the other band, around 1630 cm^{-1}, to an out-of-plane vinyl group (*61*). In CCP, the bulky Met172 residue is in close proximity to vinyl 2, and the vinyl stretching modes are found to coincide at 1623 cm^{-1} (*60*; Table 2). The Ile266 residue in *M. tuberculosis* KatG aligns with CCP Met172 and *Hm*CP Ile255 (*34*) and may cause less steric hindrance

Table 2: Assignment of Resonance Raman Bands (cm^{-1}) Observed for Ferric *M. tuberculosis* KatG, Cytochrome *c* Peroxidase (CCP), *C. cinereus* Peroxidase (CIP), Horseradish Peroxidase Isozyme A2 (HRPA2), and Tea Cationic Ascorbate Peroxidase Isoenzyme II (TcAPXII)

	KatG	CCP[a] (class I)	CIP[b] (class II)	HRPA2[c] (class III)	TcAPXII[d] (hybrid)
assignment					
ν10		1629	1631	1618, 1629, 1637	1620, 1628, 1637
ν(C=C)	1623, 1634	1620	1625	1622, 1631	1620, 1632
ν2	1571	1570	1566	1564, 1572	1572
ν3	1487, 1495, 1503	1494	1493	1485, 1492, 1503	1485, 1490, 1501
ν4	1376	1372	1371	1374	
spin state	6-c HS, 5-c HS, QS	5-c HS	5-c HS	6-c HS, 5-c HS, QS	6-c HS, 5-c HS, QS

[a] Reference *82*. [b] Reference *83*. [c] Reference *57*. [d] Reference *49*.

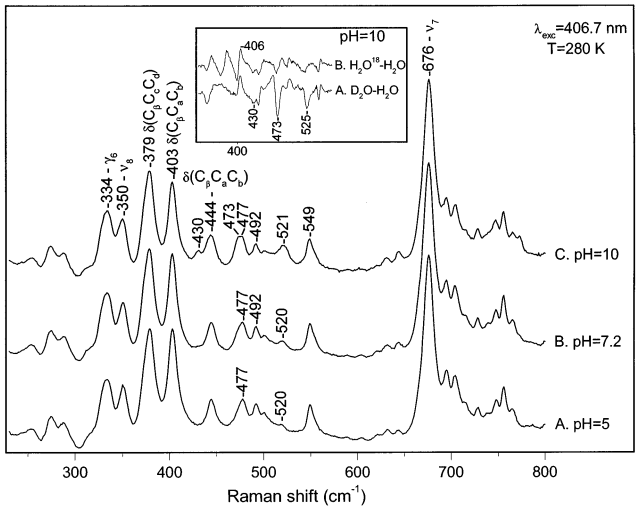

FIGURE 4: Low-frequency resonance Raman spectra of ferric wild-type KatG with 406.7 nm excitation at pH = 5 (A), pH = 7.2 (B), and pH = 10 (C). Inset: resonance Raman spectra of wild-type KatG with 406.7 nm excitation at alkaline pH in $H_2{}^{16}O$, D_2O, and $H_2{}^{18}O$ buffered solutions.

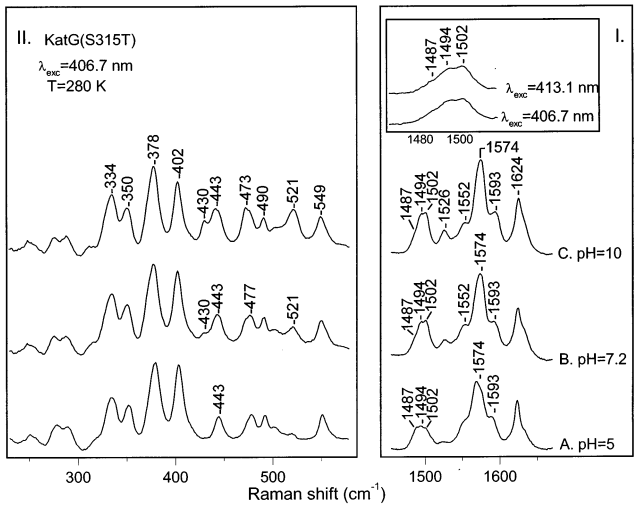

FIGURE 5: High-frequency (I) and low-frequency (II) resonance Raman spectra of KatG(S315T) with 406.7 nm excitation at pH = 5 (A), pH = 7.2 (B), and pH = 10 (C). Inset: ν_3 region of KatG(S315T) at pH = 7.2 with 406.7 and 413.1 nm excitation.

compared to Met172 in CCP, giving rise to two distinct ν(C=C) vibrations. A reproducible 1 cm^{-1} upshift is observed for the 1623 cm^{-1} band at alkaline pH. The ν_{10} modes of the 5- and 6-c HS hemes are hidden by the vinyl stretching bands, and a small intensity around 1638 cm^{-1} can be attributed to the ν_{10} mode of the QS heme spin state (*56*). Raman polarization spectra of KatG obtained with 406.7 nm excitation (see Supporting Information) support these assignments, since they reveal polarized bands for the vinyl modes (1623, 1634 cm^{-1}) and a depolarized band at 1638 cm^{-1} for the ν_{10} mode.

The low-frequency resonance Raman spectra of KatG at 280 K at acidic, neutral, and alkaline pH are shown in Figure 4. Although a full assignment of the low-frequency bands is not straightforward, a tentative assignment of several bands can be made on the basis of the heme assignment in metmyoglobin (*62*). The bands at 444 and 403 cm^{-1} are attributed to bending modes of the vinyl groups, $\delta(C_\beta C_a C_b)$. The other bands, occurring at 379, 350, and 334 cm^{-1}, are assigned to the bending mode of the propionate groups [$\delta(C_\beta C_c C_d)$], ν_8, and γ_6, respectively. The presence of an intense γ_6 band, the steady intensity of the 379 cm^{-1} band, and the absence of a band around 418 cm^{-1} are additional evidence for the absence of a 6-c LS heme (*63*). The frequency of $\delta(C_\beta C_c C_d)$ (379 cm^{-1}) is relatively high, indicating a strong hydrogen-bonding environment of the propionate groups (*64*−*66*). This is not surprising, because the *Hm*CP structure shows up to four hydrogen bonds to propionate 7 and two hydrogen bonds to propionate 6 (*31*). No changes are observed in the low-frequency region as the pH is raised from 5 to 7.2. At alkaline pH, however, the intensity of the 379 and 403 cm^{-1} bands slightly decreases, the 444 cm^{-1} band broadens, the shoulder at 473 cm^{-1} of the 477 cm^{-1} band gains intensity, and two new vibrations appear at 430 and 521 cm^{-1}. Overlapped and difference spectra that emphasize these changes are provided in the Supporting Information. The fact that the bending frequencies of the propionate groups do not change indicates that they remain firmly held by hydrogen bonds from the protein matrix. Although the new modes at 430, 473, and 521 cm^{-1} lose intensity in D_2O, they are not isotope sensitive in $H_2{}^{18}O$ (Figure 4, inset), which indicates that they cannot be due to Fe−OH or Fe−OH_2 vibrational modes. In contrast, the 379 and 403 cm^{-1} bands gain intensity in $H_2{}^{18}O$ but not in D_2O. The observation of $H_2{}^{18}O$ sensitivity of the propionate bending mode is peculiar. However, our experiments were performed at pH 10, and the C(4)=O of riboflavin can be exchanged with ^{18}O in 1 M $Na^{18}OH$ at 25 °C (*76*). Therefore, we hypothesize that, in WT KatG at pH 10, the oxygens of one of the propionate groups can be exchanged with ^{18}O, giving rise to the isotope sensitivity. We are currently conducting further experiments to test this hypothesis.

Figure 5 shows the resonance Raman spectra of ferric KatG(S315T) acquired at acidic (A), neutral (B), and alkaline (C) pH. Curve fitting to the ν_3 region at pH = 7.2 (see Supporting Information) reveals the existence of two major heme species, namely, a 5-c HS (1494 cm^{-1}) and a 5-c QS (1502 cm^{-1}) with a minor 6-c HS heme population at 1487 cm^{-1} (Table 1). The absence of bands around 565−580 nm in the electronic absorption spectrum (Figure 1) as well as the low amount of a LS heme species in the EPR data (*41*) excludes the presence of a LS heme, as already concluded for the WT enzyme. In contrast with a previous resonance Raman study, excitation at 413.1 nm does not enhance the 1502 cm^{-1} vibration (Figure 5, inset), also arguing against a LS heme species (*36*). The QS heme species is dominant in the S315T mutant (Table 1), and the 6-c HS species is almost absent, while the latter has a notable intensity in WT KatG. As the pH is raised from 7.2 to 10, the amount of the QS species does not increase, while in WT KatG an increase of the QS species is observed at alkaline pH. Polarization studies show that two vinyl stretching modes are present: one at 1623 cm^{-1} and one at 1634 cm^{-1} closely overlapped with the ν_{10} vibration of the 5-c QS heme, because its depolarization relative to the 1623 cm^{-1} mode is too low for a pure ν_{10} vibration and too high for a pure vinyl stretching mode (see Supporting Information). In the low-frequency region (Figure 5, panel II), the vibrations at 430, 473, and 521 cm^{-1} are clearly observed even at neutral pH and further enhanced at alkaline pH. The 473 and 477 cm^{-1} vibrations also gain intensity, and the propionate bending

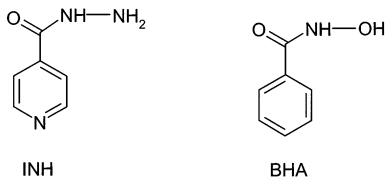

FIGURE 6: Structures of isoniazid (INH) and benzohydroxamic acid (BHA).

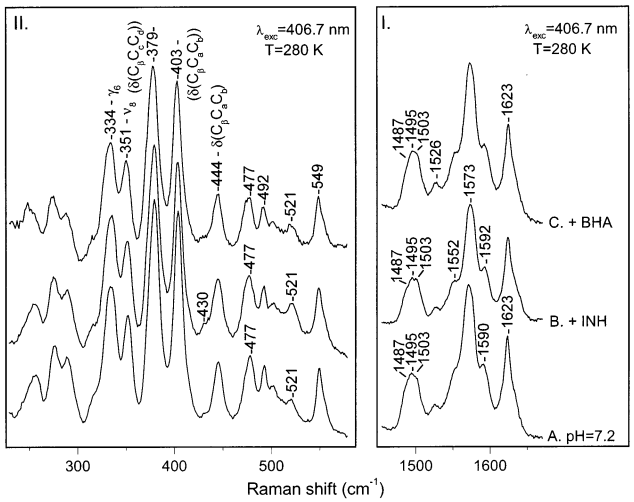

FIGURE 7: High-frequency (I) and low-frequency (II) resonance Raman spectra of ferric wild-type KatG with 406.7 nm excitation at pH = 7.2 (A) and its complex with INH (B) and BHA (C).

mode at 378 cm^{-1} slightly decreases in intensity at alkaline pH (see Supporting Information for overlapped and difference spectra). At acidic pH, a remarkable decrease of the amount of the QS (1502 cm^{-1}) is observed with a concurrent increase of the 6-c HS species (1487 cm^{-1}, Table 1). In the low-frequency region (Figure 5, panel II), there are no bands observed at 430 and 521 cm^{-1}, while the intensity of the 473 cm^{-1} band has significantly decreased.

On addition of INH to WT KatG, the Soret band blue shifts 2 nm and the CT1 band red shifts ~4 nm, indicating a slight increase in 5-c heme in the presence of the drug (data not shown). Addition of the INH structural analogue BHA (Figure 6) to WT KatG induces similar changes in the absorption spectrum, also implying an increase in the population of the 5-c heme species (data not shown). Panel I in Figure 7 compares the resonance Raman spectra of KatG and of its complexes with INH and BHA at neutral pH taken with Soret excitation. Only minor but reproducible changes occur upon the binding of INH and BHA. Curve fitting to the ν_3 region of the KatG−INH complex reveals a small decrease in the intensity of the 6-c HS species (1487 cm^{-1}) with a concurrent small increase of the intensity of the QS species (1502 cm^{-1}) with respect to resting KatG (Table 1). These small but reproducible changes noted for the ν_3 vibration are also reflected in the other vibrational modes. The ν_2 region shows a 2 cm^{-1} upshifted band, compared to resting KatG, centered at 1573 cm^{-1} with a more resolved shoulder at 1552 cm^{-1} and a 2 cm^{-1} upshifted band at 1592 cm^{-1}. The vinyl stretching vibration upshifts 1 cm^{-1}, while a slight increase in the intensity around 1638 cm^{-1}, ν_{10} of the QS heme, is observed. Binding of BHA induces the same changes in the ν_2 region. Curve fitting to the ν_3 region of the KatG−BHA complex reveals a slight increase in the

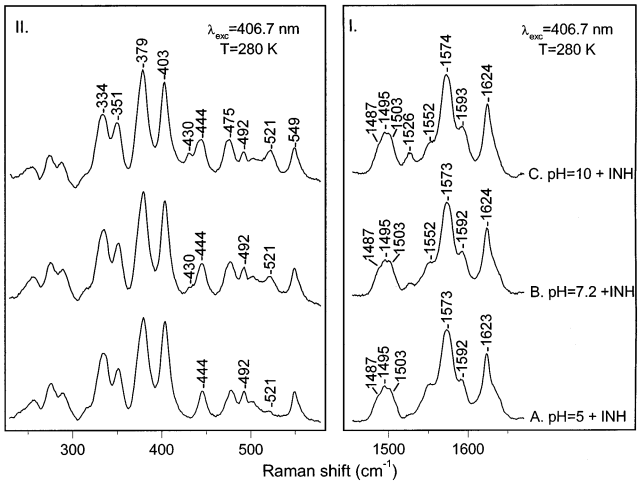

FIGURE 8: High-frequency (I) and low-frequency (II) resonance Raman spectra with 406.7 nm excitation of ferric wild-type KatG complexes with INH at pH = 5 (A), pH = 7.2 (B), and pH = 10 (C).

intensity of the 5-c HS (1495 cm^{-1}) at the expense of the 6-c HS species (1487 cm^{-1}) (Table 1), which is in contrast with the effect of INH. In the low-frequency region (Figure 7, panel II, and panel III in Supporting Information), two new vibrational modes are enhanced in the presence of INH at pH 7.2. These are the vibrations at 430 and 521 cm^{-1}, which are also observed at alkaline pH in resting KatG (Figure 4) and in the S315T mutant at pH = 7.2 (Figure 5). The same modes are weakly enhanced in the presence of BHA.

Soret-excited resonance Raman spectra of the INH complexes of KatG at acidic, neutral, and alkaline pH are shown in Figure 8. At acidic pH, the 6-c HS (1487 cm^{-1}) species loses intensity upon addition of INH while the 5-c HS (1495 cm^{-1}) and QS (1503 cm^{-1}) slightly gain intensity (Table 1, Figures 3 and 8). The formation of a minor amount of 6-c LS heme upon addition of the drug cannot be excluded as indicated by the shoulders at 1506 and 1640 cm^{-1}, which could be tentatively assigned to the ν_3 and ν_{10} modes of a LS heme, respectively. The band centered at 1570 cm^{-1} in ligand-free KatG (pH 5) upshifts 3 cm^{-1} in the presence of the drug while the 1552 cm^{-1} band becomes more resolved and the 1590 cm^{-1} mode upshifts. In the low-frequency region, no changes are observed with respect to WT KatG at pH 5 (Figures 4 and 8). At alkaline pH, addition of the drug does not induce any further changes in either the high- or the low-frequency region compared to the WT enzyme at pH 10 and its INH complex at pH 7.2.

Figure 9 compares the resonance Raman spectrum of WT KatG (A) to that of fresh WT KatG (B), the S315T mutant (C), and WT KatG with its 10-fold isoniazid complex (D) in both high- and low-frequency regions at neutral pH. It is clearly shown that the amount of the QS species is increased in the mutant enzyme with a concurrent decrease of the 6-c HS species and a slight increase of the 5-c HS species compared to the WT enzyme (Table 1). Also, the amount of the QS in fresh WT enzyme is comparable to that in the mutant enzyme (Table 1). In the low-frequency region, the bands at 473 and 521 cm^{-1} are enhanced in KatG(S315T) while a new band appears at 430 cm^{-1}. For comparison, the spectra of WT KatG in the presence of INH at pH 7.2 are shown. On addition of INH to KatG(S315T), no further

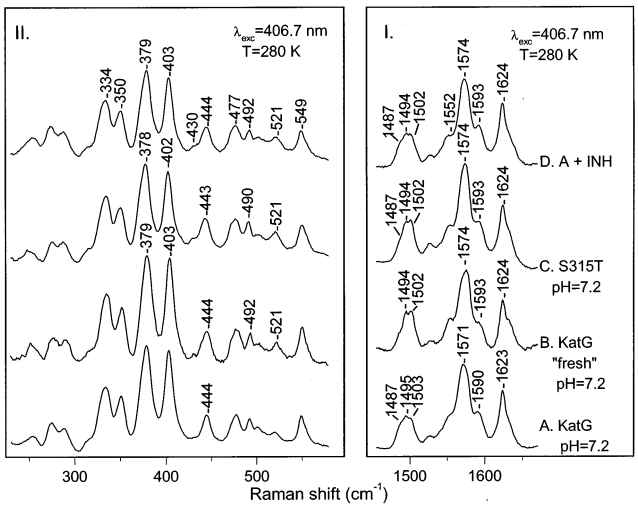

FIGURE 9: High-frequency (I) and low-frequency (II) resonance Raman spectra of ferric wild-type KatG with 406.7 nm excitation at pH = 7.2 (A), of ferric wild-type fresh KatG (B), of KatG(S315T) at pH = 7.2 (C), and the WT KatG−INH complex (D).

changes are observed (data not shown). It should be emphasized that the resonance Raman spectra of fresh WT KatG and KatG(S315T) are nearly identical. The QS state dominates in both preparations, and the enhancement of the low-frequency vibrations is observed in both fresh WT and mutant KatG. It should be noted that both the QS population and the intensity of the low-frequency vibrations decrease in WT KatG after storage, while they remain stable in the S315T mutant.

DISCUSSION

Coordination and Spin States of the Heme in Wild-Type KatG and KatG(S315T). The location of the oxidation state marker band, ν_4, at 1376 cm^{-1} in the wild-type and mutant KatG is typical of a ferric heme, and the ν_3 region reveals the existence of three heme spin states with characteristic frequencies at 1487, 1495, and 1503 cm^{-1} in both WT KatG and KatG(S315T). The 1487 and 1495 cm^{-1} vibrations are assigned to a 6-c HS and a 5-c HS ferric heme, respectively (*50*). The ν_3 vibration at 1503 cm^{-1} is assigned to a 5-c QS heme and not a 6-c LS heme on the basis of electronic absorption and EPR spectra (*41*) and our resonance Raman data obtained with 406.7 and 413.1 nm excitation. The relative contributions of these vibrations are different for the two enzymes (Table 1). KatG(S315T) has significantly more 5-c QS heme at the expense of 6-c HS heme compared to WT KatG. Fresh WT KatG, however, has a population of heme species very similar to KatG(S315T) (Figure 9, Table 1). The ν_3 vibration of the 6-c HS heme is slightly higher than for a typical 6-c HS heme, and a small admixture of an intermediate state ($S = {}^3/_2$) cannot be excluded (*67*). On the basis of EPR and resonance Raman experiments, admixture of an intermediate state has been proposed for the 6-c HS heme of the KatG−chloride complex, which has a ν_3 vibration at 1489 cm^{-1} (*41*). Higher frequencies for certain skeletal vibrations have also been reported for the 6-c complex of recombinant horseradish peroxidase C (HRP-C) and some mutants, as well as for BHA complexes of some peroxidases (*63*, *67*).

The 5-c QS results from the admixture of high ($S = {}^5/_2$) and intermediate ($S = {}^3/_2$) heme spin states (*53*, *54*). Owing to only partial occupation of the $d_{x^2-y^2}$ orbitals, the in-plane bonds to the heme iron are shortened in the QS state compared to the HS state, and the core size in the QS state is expected to be similar to that of a LS heme (*55*). Accordingly, the core-size marker band frequencies are also expected to be similar to those of the LS form (*51*). In support of our assignment, EPR results at 4 K revealed a rhombic signal characteristic of 5-c heme (g_1, g_2, g_3 = 6.3, 5.2, ~2), of which the intensity correlates with the intensity of the 1503 cm^{-1} band in various KatG samples. More importantly, comparison of freshly isolated KatG and KatG after storage demonstrated a decrease in the intensity of this EPR signal concomitant with a decrease in the QS heme ν_3 band intensity (*41*). Furthermore, the mutant KatG(S315T) exhibits more QS heme in resonance Raman spectra at room temperature and a greater intensity of the same EPR signal at 4 K compared to WT KatG. These observations provide strong support for the assignment of the 1503 cm^{-1} band to a 5-c QS heme rather than to a 6-c LS heme (*41*). Since heme spin state populations may be affected at cryogenic temperatures (*68*), low-temperature resonance Raman experiments are planned to corroborate the correlation between the EPR and Raman results.

The observation of a QS heme state in a class I catalase−peroxidase is rather striking, because it has been observed only in class III peroxidases, barley peroxidase and HRPA2 at both room and low temperature (*56*, *57*), in soybean peroxidase (*59*), and in HRP-C at low temperature (*50*, *58*). The class III tea cationic ascorbate peroxidase II, which has been shown to combine spectroscopic characteristics and substrate specificities of both class I and class III peroxidases, also has a QS heme (*49*). Our observation of a QS heme in *M. tuberculosis* KatG is the first report of a quantum mechanically mixed spin heme species in a class I peroxidase, and this observation is different from that in an earlier resonance Raman study of *M. tuberculosis* KatG and a more recent study of *Synechocystis* KatG (*36*, *42*). The origin of these differences is not clear but may be related to differences in overexpression, isolation, or purification procedures. Potential factors that affect the stabilization of the QS heme will be addressed below. The absence of an endogenous strong field ligand at the sixth ligand position in the crystal structure of *Hm*CP is in agreement with the absence of a 6-c LS heme (*31*). Furthermore, the constant relative abundance of 5-c HS heme is consistent with EPR results, and we suggest here that this observation may reflect differences between the heme pocket within each monomer of the dimer such that one is flexible while the other is not. The X-ray structure of *Hm*CP also suggests that the two heme pockets are different (*31*).

Effect of INH Binding on the Heme Spin State Distribution. At physiological pH, the heme spin state distribution in WT KatG is about equal for the three different spin states, while in KatG(S315T) the QS state is favored at the expense of the 6-c HS state (see Table 1). Addition of INH to WT KatG changes the heme spin state distribution slightly in favor of the 5-c QS state at the expense of 6-c HS species. The addition of INH (500-fold excess) to KatG(S315T) has no significant effect on its heme spin state distribution. The intensity changes observed in the resonance Raman spectra upon addition of INH are in agreement with those previously described for the electronic absorption spectra and resonance

Raman experiments (*35*, *38*). The minor but reproducible changes induced by INH binding indicate that INH does not interact directly with the heme iron. This is consistent with NMR relaxation studies, which estimated the Fe−INH amide nitrogen distance at ~4 Å for both proteins (*38*, *40*).

Since a crystal structure of INH-bound *M. tuberculosis* KatG is not yet available, we took advantage of another organic ligand, benzohydroxamic acid (BHA), to investigate the enzyme−substrate interactions. BHA has been extensively used as a convenient probe for the aromatic donor binding site in peroxidases. INH and BHA have similar size and functional groups (Figure 6), and the binding affinities of BHA and INH for KatG are very similar (data not shown), both in the micromolar range, comparable to that of BHA for the class III peroxidase HRP-C (*69*). A similar binding mode has been proposed for BHA and INH to HRP-C despite its low affinity for INH (K_d = 1 mM) (*70*). In HRP-C, BHA binding induces the formation of a 6-c QS heme, most likely by stabilizing a water molecule near the heme iron (*67*). In contrast, addition of BHA to WT KatG results in a small increase of the 5-c HS state at the expense of the 6-c HS species (Table 1). From this observation, we propose that BHA and INH displace the water molecule more in KatG than BHA does in HRP-C, giving rise to the interconversion of 6-c HS heme to 5-c HS and 5-c QS hemes, respectively. This is consistent with previously reported data where INH binding has been suggested to promote changes in the distal pocket that include loss of coordinated water (*38*). This idea is supported by the distance between the amide nitrogen of BHA and the heme iron in HRP-C, which is larger than that of the INH amide nitrogen to the heme iron in KatG, about 5.6 Å versus about 4 Å, respectively (*43*, *40*).

Stabilization of the Quantum Spin Heme. Although fresh WT KatG contains the same amount of QS heme as KatG(S315T), the purified WT enzyme contains a smaller but stable amount of a QS heme (Table 1). An increase in the population of the QS heme in WT KatG is observed on binding of INH or raising the pH and in the S315T mutant. Since the proximal ligand of the KatG heme has an imidazolate character (*31*, *36*; data not shown) we rule out that the QS state in KatG is due to a weak proximal ligand as previously proposed for model compounds (*71*). Our results support the more recently proposed mechanism for the stabilization of the QS heme state, the saddling of the heme (*55*, *72*). Since the effect of INH on the stability of the QS heme is relatively small, we will focus our discussion on the effect of pH and the S315T mutation on QS heme stability.

Both WT KatG and KatG(S315T) show a pH dependence of the population of the QS heme state. In WT KatG, the increase in the population of 5-c QS heme and the concomitant loss of 6-c HS heme occurs between pH 7.2 and pH 10, while it occurs between pH 5 and pH 7.2 in the S315T mutant (Table 1). Although we cannot rule out that we are measuring a process that occurs outside of the heme pocket, there are several amino acid residues of interest inside the heme pocket that may be involved in the transition from 6-c HS to 5-c QS heme. The fact that mutation of Ser315 has an effect on this transition and makes a hydrogen bond with the heme 7-propionate (*31*) suggests that the orientation of the heme 7-propionate plays a role in this transition. By using the *Hm*CP heme pocket as a model for *M. tuberculosis* KatG

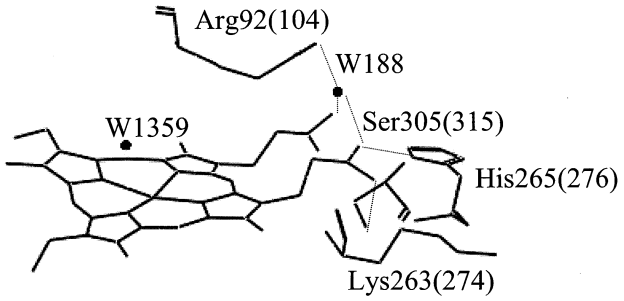

FIGURE 10: Active site of *Hm*CP based on the X-ray crystal structure (*31*). The labels between parentheses are the residues of *M. tuberculosis* KatG based on sequence homology with CCP and *Hm*CP.

(*31*), we can identify three residues that form hydrogen bonds to the heme propionate groups: Ser315, His276, and Lys274 (Figure 10). Furthermore, there is an extensive network of water molecules in the distal pocket in peroxidases and *Hm*CP and, presumably, in KatG. In *Hm*CP, water molecule 188 forms a hydrogen bond between Arg92 and the heme propionates (Figure 10). It is expected that the pK_as of the protons involved in hydrogen bonding are raised, because they are stabilized by the hydrogen bonds. In WT KatG, the largest increase in 5-c QS population occurs in the pH range from 7.2 to 10, which indicates that the pK_a of the group involved in this process is within this range. Ser and Lys have pK_a values above 9, which will be only higher in their hydrogen-bonded form. The pK_a value of the imidazole proton of histidine is 6.0 in water, and stabilization of this proton by hydrogen bonding can raise its pK_a within the pH range that is observed for 6-c HS to 5-c QS heme transition in WT KatG. Therefore, we propose that His276 plays an important role in this transition. The 6-c HS to 5-c QS heme transition in KatG(S315T) occurs between pH 5 and pH 7.2, which is closer to the normal pK_a of His. We propose that the S315T mutation weakens the hydrogen bond between His276 and the heme 7-propionate group due to steric hindrance of the Thr methyl group, thereby bringing its pK_a closer to its normal value.

The high frequency of the propionate bending mode $\delta(C_\beta C_c C_d)$ at 379 and 378 cm^{-1} in WT KatG and KatG(S315T), respectively, is in agreement with the presence of a strong hydrogen-bonding environment most likely involving the Ser315, His276, and Lys274 residues that firmly anchor the heme moiety into the protein matrix. Removal of one hydrogen bond by deprotonation of His276 is expected to result in lowering the frequency of the $\delta(C_\beta C_c C_d)$ mode (*64*−*66*, *73*). Such a change in hydrogen bonding to the heme 7-propionate could result in an increase in nonplanar heme deformation, which leads to formation of the 5-c QS heme state due to heme saddling (*72*). Although we observe a small decrease in the intensity of the $\delta(C_\beta C_c C_d)$ mode, we do not observe the expected frequency decrease when the population of 5-c QS heme changes. In the case of KatG, however, the heme 7-propionate accepts up to four hydrogen bonds, and the removal of one hydrogen bond may not be as dramatic, because the remaining hydrogen bonds will still firmly secure the heme propionate group in the protein matrix. Furthermore, changes in one of the two hydrogen bonds to the heme 7-propionate in Mb does not always change the frequency of the

$\delta(C_\beta C_c C_d)$ mode (*74*). Therefore, our proposal that the frequency of the $\delta(C_\beta C_c C_d)$ mode in WT KatG would not change when only one out of four hydrogen bonds is altered is not unprecedented. The small decrease in the intensity of this vibration may actually indicate a reorientation of the propionate involving the $C_\beta C_c C_d C$ torsional angle, inducing more nonplanarity onto the heme plane while keeping the carboxylate group firmly anchored to the protein matrix. Nonplanar heme deformation due to an increase in pH and the S315T mutation is also supported by the observation of three new low-frequency vibrations, of which the origin will be discussed in the next section. We propose that removal of one hydrogen bond, presumably between His276 and the heme 7-propionate, induces more nonplanar heme deformation, e.g., saddling of the heme, which has been associated with stabilization of QS heme (*72*). Interactions between the heme propionates and the protein have already been reported to influence the heme conformation in ferricytochromes c_3 (*75*), and the recent crystal structure of *Hm*CP also shows a strongly deformed, nonplanar heme, in agreement with our proposal (*31*). A combination of mutagenesis, EPR, and resonance Raman studies is planned to sort out the effect of specific residues on the heme spin state.

Origin and Enhancement of Low-Frequency Vibrations. At physiological pH, the S315T mutation and addition of INH to WT KatG result in enhancement of the vibrations observed at 473 and 521 cm^{-1} and the appearance of a mode at 430 cm^{-1}, while addition of INH to the mutant also induces an increase in the intensity of these vibrations. A significant increase in the intensities of these vibrations occurs by increasing the pH from 5 to 10 in both WT KatG and KatG(S315T). The enhanced vibrations have frequencies that have been associated with Fe−OH_2 and Fe−OH complexes (*70*, *71*). Although our experiments carried out in D_2O show that these vibrations are isotope sensitive, our experiments in $H_2{}^{18}O$ did not show any isotope sensitivity of these modes, which indicates that they are associated with neither Fe−OH nor Fe−OH_2 vibrational modes. Furthermore, when a significant amount of 6-c HS is present in WT and KatG(S315T) at pH 5, the vibrations at 430, 473, and 521 cm^{-1} are not observed. Their isotope sensitivity in D_2O may be related to deuteration of amino acids that donate hydrogen bonds to the heme propionate groups.

The exact composition of the enhanced vibrational modes associated with these low-frequency bands is not known, but a tentative assignment can be made. On the basis of resonance Raman data of tetragonal and triclinic crystalline forms of nickel octaethylporphyrin, the band at 521 cm^{-1} could be equivalent to a δ_2 [$\delta(C_\beta C_1 C_2)$sym] mode, the 473 cm^{-1} could be equivalent to a δ_4 [($\delta(C_\beta C_1 C_2)$sym], and the one at 430 cm^{-1} to a δ_1 [$\delta(C_\beta C_1 C_2)$asym] mode, the symmetric and asymmetric ethyl bending modes, respectively (*77*). In the tetragonal crystals, the ruffled porphyrin ring causes the enhancement of the out-of-plane modes. Pyrrole folding modes have also been suggested for vibrations between 500 and 600 cm^{-1} (*77*). These vibrations would also be enhanced when the heme is nonplanar. Furthermore, the lack of vibrations at 430, 473, and 521 cm^{-1} at acidic pH is consistent with previously reported observations on Ni-Cyt *c* (*78*) that at lower pH a decrease in the amount of the nonplanar relative to the planar porphyrin conformer occurs. The increase in the intensity of the 430 cm^{-1} mode occurs concomitant with a decrease in the intensity of the 403 cm^{-1} vibration. Therefore, appearance of the 430 cm^{-1} mode may be due to a transition from an in-plane vinyl conformer at 403 cm^{-1} to an out-of-plane conformer at 430 cm^{-1} (*62*, *79*), induced by the heme deformation, whereas a pyrrole folding mode is more likely the assignment for the 521 cm^{-1} mode, because its frequency is too high for a vinyl or a propionate bending vibration.

Table 3: Comparison of Percentage of QS Heme and Intensity of the 521 cm^{-1} Vibration after Normalization of Spectra on the ν_7 Vibration

pH	WT QS	WT 521 cm^{-1}	WT + INH QS	WT + INH 521 cm^{-1}	S315T QS	S315T 521 cm^{-1}
5	29	1.4	35	1.7	21	1.6
7.2	32	2.9	37	5.6	49	7.4
10	40	8.3	39	9.9	51	16.8

In contrast with the stabilization of the 5-c QS heme, which has been proposed to correlate with a saddling deformation (*55*, *72*), the enhancement of the low-frequency vibrations has been associated with a ruffling deformation of the heme plane (*77*). Despite the difference in the heme deformation, the same interactions between heme and the KatG heme pocket residues that we identified for stabilization of the 5-c QS heme in WT KatG are most likely responsible for the enhancement of the vibrations at 521, 473, and 430 cm^{-1}. Changes in the hydrogen bonding of the propionate groups that are induced by INH binding, alkaline pH, and the S315T mutation can result in nonplanar heme deformations as discussed above. Therefore, the same interactions can lead to stabilization of 5-c QS heme and enhancement of the low-frequency vibrations, but the type of heme deformation is most likely different, i.e., saddling and ruffling, respectively. The most important observation is that the low-frequency vibrations are indicative of a conformational change of the heme cofactor and the heme pocket, which occurs on INH binding to WT KatG, on mutation of Ser315 to Thr at physiological pH, and on increasing pH.

Relation between QS Heme and Low-Frequency Vibrations. In the previous sections, we argued that the enhancement of the low-frequency vibrations and the stabilization of the QS heme are associated with different heme deformations, i.e., ruffling and saddling, respectively. A correlation between the QS species and the low-frequency vibrations can be ruled out. Between pH 7.2 and pH 10, the vibrations at 430 and 521 cm^{-1} become strongly enhanced in KatG(S315T), while the population of the QS species does not change. A comparison of the percentage of QS and the intensity of the 521 cm^{-1} mode, which is given in Table 3, emphasizes this conclusion. This is consistent with the observation that ruffling does not have any significant influence on stabilizing the QS state (*55*). A correlation with the 6-c HS heme can also be ruled out. This heme species has its largest population at pH 5, while the low-frequency vibrations are not observed at this pH. Finally, the 5-c HS heme does not show any correlation either. When the pH is raised from 7.2 to 10 in both WT KatG and KatG(S315T), the population of 5-c HS heme remains stable (Table 1), while the intensity of the low-frequency vibrations increases significantly. Therefore, there is no direct correlation between the enhancement of the low-frequency vibrations and any of the three heme species, even though the QS heme may

result from similar conformational changes in the heme pocket.

Mode of Inhibition of INH Oxidation in KatG(S315T). Two important differences between WT KatG and KatG(S315T) should be pointed out. First, the QS heme population in KatG(S315T) is rather stable and does not vary much when the enzyme ages (Table 1). In fresh WT KatG, the population of QS can be as high as in KatG(S315T), but when WT KatG ages, the population of the QS heme decreases to a stable population of about 32% (*41*; Table 1). Second, fresh WT KatG shows significant enhancement of the 430, 473, and 521 cm^{-1} vibrations, which lose intensity as the enzyme ages. In contrast, the intensity of these vibrations is not affected when KatG(S315T) ages. Therefore, the S315T mutation seems to stabilize the heme pocket conformation in KatG such that a nonplanar heme conformation is favored.

Since the QS heme is the major heme species in fresh WT KatG, we rule out that the QS state is responsible for the inhibition of INH oxidation in KatG(S315T). Recently, it has been proposed that the QS state in HRP-C constitutes the heme reactivity (*80*). Furthermore, QS heme states have also been observed in situ (*81*), providing further support that the QS heme can be a native functional state of a heme enzyme. The appearance of the low-frequency vibrations in fresh WT KatG indicates that both WT and mutant enzyme share similar heme and heme pocket conformations. Therefore, we suggest that the inhibition of INH oxidation does originate from neither a modification of the active site nor an alteration in the chemical reactivity due to the QS heme. Actually, the S315T mutation seems to preserve the active site structure of KatG, while it is subject to a slow conformational change over time in the WT enzyme (*41*), resulting in a more planar heme conformation. To explain the inhibition of INH oxidation, the S315T mutation has to induce a structural change in another part of the enzyme. On the basis of the crystal structure of *Hm*CP, the heme in KatG is buried inside the N-teminal domain, and substrate access to the active site is through a narrow, cylindrical channel which is ~3.5 Å in diameter at Ser305 (Ser315 in KatG) around the heme iron, and its width increases from Ser305 to the molecular surface (*31*). Therefore, our results and conclusions support the proposal that the loss of INH activation in the S315T mutant may arise from steric hindrance induced by the extra methyl group of the Thr residue, which is situated along the access channel and consequently blocks the entrance to the heme distal site (*31*), rather than from modification of the active site of the enzyme (*37*).

Concluding Remarks. The combined analysis of UV−vis and resonance Raman spectroscopy revealed the existence of a QS heme state, besides 6-c HS and 5-c HS heme states, in both WT KatG and KatG(S315T). The population of the QS species is dominant and stable in KatG(S315T) at physiological pH, while it decreases in WT KatG to about 32% after purification. The QS heme becomes more prominent in WT KatG after addition of INH at physiological pH and by raising the pH. Since the relative population of the 5-c HS heme remains constant, we believe that this may reflect differences between the heme pocket within each monomer of the dimer. Besides the QS heme, two new low-frequency vibrations are observed at 430 and 521 cm^{-1} in KatG(S315T), which are also present in fresh WT KatG. The enhancement of these vibrations may be associated with a ruffled heme plane, and the stabilization of the QS may be due to saddling of the heme, which suggests that the heme pocket conformation in KatG(S315T) and fresh WT KatG is different from aged WT KatG. Furthermore, we propose that the hydrogen bond between His276 and the heme 7-propionate can be titrated to stabilize the QS state and to enhance the low-frequency vibrations due to formation of a more nonplanar heme conformation. We rule out that neither the QS heme nor the heme pocket conformation causes the inhibition of INH oxidation in *M. tuberculosis* KatG(S315T). Finally, our data support the proposal that the inhibition of INH oxidation by the S315T mutant arises from the steric hindrance introduced by the methyl group of the Thr residue, which prevents INH to access the distal heme pocket.

SUPPORTING INFORMATION AVAILABLE

Curve fitting of the ν_3 region of the resonance Raman spectra of WT KatG and KatG(S315T), overlapped resonance Raman spectra of WT KatG and KatG(S315T) in the low-frequency region, and polarized resonance Raman spectra of WT KatG and KatG(S315T) at pH = 7.2 with 406.7 nm excitation. This material is available free of charge via the Internet at http://pubs.acs.org.

REFERENCES

1. World Health Organization (2002) World Health Report.
2. Fox, H. H. (1951) *Chem. Eng. News 29*, 3963−3964.
3. Banerjee, A., Dubnau, E., Quemard, A., Balasubramanian, V., Um, K. S., Wilson, T., Collins, D., deLisle, G., and Jacobs, W. R., Jr. (1994) *Science 263*, 227−230.
4. Quemard, A., Sacchettini, J. C., Dessen, A., Vilcheze, C., Bittman, R., Jacobs, W. R., Jr., and Blanchard, J. S. (1995) *Biochemistry 34*, 8235−8241.
5. Mdluli, K., Slayden, R. A., Zhu, Y., Ramaswamy, S., Pan, X., Mead, D. D., Musser, J. M., and Barry, C. E., III (1998) *Science 280*, 1607−1610.
6. Johnsson, K., and Schultz, P. G. (1994) *J. Am. Chem. Soc. 116*, 7425−7426.
7. Quemard, A., Dessen, A., Sugantino, M., Jacobs, W. R., Jr., Sacchettini, J. C., and Blanchard, J. S. (1996) *J. Am. Chem. Soc. 118*, 1561−1562.
8. Basso, L. A., Zheng, R., and Blanchard, J. S. (1996) *J. Am. Chem. Soc. 118*, 11301−11302.
9. Johnson, K., King, D. S., and Schultz, P. G. (1995) *J. Am. Chem. Soc. 117*, 5009−5010.
10. Basso, L. A., Zheng, R., Musser, J. M., Jacobs, W. R., Jr., and Blanchard, J. S. (1998) *J. Infect. Dis. 178*, 769−775.
11. Wengenack, N. L., Jensen, M. P., Rusnack, F., and Stern, M. K. (1999) *Biochem. Biophys. Res. Commun. 256*, 485−487.
12. Musser, J. M. (1995) *Clin. Microbiol. Rev. 8*, 496−514.
13. Heym, B., Alzari, P. M., Honore, N., and Cole, S. T. (1995) *Mol. Microbiol. 15*, 235−245.
14. Musser, J. M., Kapur, V., Williams, D. L., Kreiswirth, B. N., van Soolingen, D., and van Embden, J. D. A. (1996) *J. Infect. Dis. 173*, 196−202.
15. Marttila, H. J., Soini, H., Eerola, E., Vyshnevakaya, E., Vyshnevskiy, B. I., Otten, T. F., Vasilyef, A. V., and Viljanen, M. K. (1998) *Antimicrob. Agents Chemother. 42*, 2443−2445.
16. Heym, B., Honore, N., Truffot-Pernot, C., Banerjee, A., Schurra, C., Jacobs, W. R., Jr., van Embden, J. D., Grosset, J. H., and Cole, S. T. (1994) *Lancet 344*, 293−298.
17. Rouse, D. A., DeVito, J. A., Li, Z., Byer, H., and Morris, S. L. (1996) *Mol. Microbiol. 22*, 583−592.
18. Victor, T. C., Pretorius, G. S., Felix, J. V., Jordan, A. M., van Helden, P. D., and Eisenach, K. D. (1996) *Antimicrob. Agents Chemother. 40*, 1572.

19. Heym, B., and Cole, S. T. (1997) *Int. J. Antimicrob. Agents 8*, 61−70.
20. Haas, W. H., Schilke, K., Brand, J., Amthor, B., Weyer, K., Fourie, P. B., Betzel, G., Sticht-Groh, V., and Bremer, H. J. (1997) *Antimicrob. Agents Chemother. 41*, 1601−1603.
21. Welinder, K. G. (1992) *Curr. Opin. Struct. Biol. 2*, 388−393.
22. Welinder, K. G. (1991) *Biochim. Biophys. Acta 1080*, 215−220.
23. Heym, B., Zhang, Y., Poulet, S., Young, D., and Cole, S. (1993) *J. Bacteriol. 175*, 4255−4259.
24. Johnsson, K., Froland, W. A., and Schultz, P. G. (1997) *J. Biol. Chem. 272*, 2834−2840.
25. Magliozzo, R. S., and Marcinkeviciene, J. A. (1996) *J. Am. Chem. Soc. 118*, 11303−11304.
26. Marcinkeviciene, J. A., Magliozzo, R. S., and Blanchard, J. S. (1995) *J. Biol. Chem. 270*, 22290−22295.
27. Magliozzo, R. S., and Marcinkeviciene, J. A. (1997) *J. Biol. Chem. 272*, 8867−8870.
28. Wengenack, N. L., Uhl, J. R., St. Amand, A. L., Tomlinson, A. J., Benson, L. M., Naylor, S., Kline, B. C., Cockerill, F. R., and Rusnak, F. (1997) *J. Infect. Dis. 176*, 722−727.
29. Yamada, Y., Saijo, S., Sato, T., Igarashi, N., Usui, H., Fujiwara, T., and Tanaka, N. (2001) *Acta Crystallogr. D57*, 1157−1158.
30. Carpena, X., Guarne, A., Ferrer, J. C., Alzari, P. M., Fita, I., and Loewen, P. C. (2002) *Acta Crystallogr. D58*, 853−855.
31. Yamada, Y., Fujiwara, T., Sato, T., Igarashi, N., and Tanaka, N. (2002) *Nat. Struct. Biol. 9*, 691−695.
32. Finzel, B. C., Poulos, T. L., and Kraut, J. (1984) *J. Biol. Chem. 259*, 13027−13036.
33. Patterson, W. R., and Poulos, T. L. (1995) *Biochemistry 34*, 4331−4341.
34. Zamocky, M., Regelsberger, G., Jakopitsch, C., and Obinger, C. (2001) *FEBS Lett. 492*, 177−182.
35. Chouchane, S., Lippai, I., and Magliozzo, R. S. (2000) *Biochemistry 39*, 9975−9983.
36. Lukat-Rodgers, G. S., Wengenack, N. L., Rusnak, F., and Rodgers, K. R. (2000) *Biochemistry 39*, 9984−9993.
37. Lukat-Rodgers, G. S., Wengenack, N. L., Rusnak, F., and Rodgers, K. R. (2001) *Biochemistry 40*, 7149−7157.
38. Wengenack, N. L., Todorović, S., Yu, L., and Rusnak, F. (1998) *Biochemistry 37*, 15825−15834.
39. Wengenack, N. L., Hoard, H. M., and Rusnak, F. (1999) *J. Am. Chem. Soc. 121*, 9748−9749.
40. Todorović, S., Juranić, N., Macura, S., and Rusnak, F. (1999) *J. Am. Chem. Soc. 121*, 10962−10966.
41. Chouchane, S., Girotto, S., Kapetanaki, S., Schelvis, J. P. M., Yu, S., and Magliozzo, R. S. (2003) *J. Biol. Chem. 278*, 8154−8162.
42. Heering, H. A., Indiani, C., Regelsberger, G., Jakopitsch, C., Obinger, C., and Smulevich, G. (2002) *Biochemistry 41*, 9237−9247.
43. Henriksen, A., Schuller, D. J., Meno, K., Welinder, K. G., Smith, A. T., and Gajhede, M. (1998) *Biochemistry 37*, 8054−8060.
44. Loewen, P. C., and Stauffer, G. V. (1990) *Mol. Gen. Genet. 224*, 147−151.
45. Sanger, F., Nicklen, S., and Coulson, A. R. (1977) *Proc. Natl. Acad. Sci. U.S.A. 74*, 5463−5467.
46. Abe, M., Kitagawa, T., and Kyogoku, Y. (1978) *J. Chem. Phys. 69*, 4526−4534.
47. Choi, S., and Spiro, T. G. (1983) *J. Am. Chem. Soc. 105*, 3683−3692.
48. Choi, S., Lee, J. J., Wei, Y. H., and Spiro, T. G. (1983) *J. Am. Chem. Soc. 105*, 3692−3707.
49. Heering, H. A., Jansen, M. A. K., Thorneley, R. N. F., and Smulevich, G. (2001) *Biochemistry 40*, 10360−10370.
50. Dunford, H. B. (1999) in *Heme Peroxidases*, pp 135−143, Wiley-VCH, New York.
51. Spiro, T. G. (1988) in *Biological Applications of Raman Spectroscopy* (Spiro, T., Ed.) pp 1−38, John Wiley & Sons, New York.
52. Maltempo, M. M., Moss, T. H., and Cusanovich, M. A. (1974) *Biochim. Biophys. Acta 342*, 290−305.
53. Maltempo, M. M. (1974) *J. Chem. Phys. 61*, 2540−2547.
54. Fujii, S., Yoshimura, T., Kamada, H., Yamaguchi, S., Suzuki, S., Shidara, S., and Takakuwa, S. (1995) *Biochim. Biophys. Acta 1251*, 161−169.
55. Howes, B. D., Schiødt, C. B., Welinder, K. G., Marzocchi, M. P., Ma, J.-G., Zhang, J., Shelnutt, J. A., and Smulevich, G. (1999) *Biophys. J. 77*, 478−492.
56. Smulevich, G., Feis, A., Indiani, C., Becucci, M., and Marzocchi, M. P. (1999) *JBIC, J. Biol. Inorg. Chem. 4*, 39−47.
57. Feis, A., Howes, B. D., Indiani, C., and Smulevich, G. (1998) *J. Raman Spectrosc. 29*, 933−938.
58. Nissum, M., Feis, A., and Smulevich, G. (1998) *Biospectroscopy 4*, 355−364.
59. Bedard, P., and Mabrouk, P. A. (1997) *Biochem. Biophys. Res. Commun. 240*, 65−67.
60. Smulevich, G. (1998) *Biospectroscopy 4*, S3−S17.
61. Kalsbeck, W. A., Robertson, D. E., Pandey, R. K., Smith, K. M., Dutton, P. L., and Bocian, D. F. (1996) *Biochemistry 35*, 3429−3438.
62. Hu, S., Smith, K. M., and Spiro, T. G. (1996) *J. Am. Chem. Soc. 118*, 12638−12646.
63. Smulevich, G., Mauro, J. M., Fishel, L. A., English, A. M., Kraut, J., and Spiro, T. G. (1988) *Biochemistry 27*, 5477−5485.
64. Friedman, J. M., and Peterson, E. (1996) in *Proceedings of the XIVth International Conference on Raman Spectroscopy* (Asher, S. A., and Stein, P. B., Eds.) p 428, John Wiley & Sons, New York.
65. Gottfried, D. S., Peterson, E. S., Sheikh, A. G., Wang, J., Yang, M., and Friedman, J. M. (1996) *J. Phys. Chem. 100*, 12034−12042.
66. Cerda-Colón, J. F., Silfa, E., and López-Garriga, J. (1998) *J. Am. Chem. Soc. 120*, 9312−9317.
67. Indiani, C., Feis, A., Howes, B. D., Marzocchi, M. P., and Smulevich, G. (2000) *J. Am. Chem. Soc. 122*, 7368−7376.
68. Evangelista-Kirkup, E., Crisanti, M., Poulos, T. L., and Spiro, T. G. (1985) *FEBS Lett. 190*, 221−226.
69. Schonbaum, G. R. (1973) *J. Biol. Chem. 248*, 502−511.
70. Aitken, S. M., Turnbull, J. L., Percival, M. D., and English, A. M. (2001) *Biochemistry 40*, 13980−13989.
71. Scheidt, W. R., and Reed, C. A. (1981) *Chem. Rev. 81*, 543−555.
72. Cheng, R.-J., Chen, P.-Y., Gau, P.-R., Chen, C.-C., and Peng, S.-M. (1997) *J. Am. Chem. Soc. 119*, 2563−2569.
73. Lloyd, E., Burk, D. L., Ferrer, J. C., Maurus, R., Doran, J., Carey, P. R., Brayer, G. D., and Mauk, A. G. (1996) *Biochemistry 35*, 11901−11912.
74. Peterson, E. S., Friedman, J. M., Chien, E. Y., and Sligar, S. G. (1998) *Biochemistry 37*, 12301−12319.
75. Ma, J.-G., Zhang, J., Franco, R., Jia, S.-L., Moura, I., Moura, J. J. G., Kroneck, P. M. H., and Shelnutt, J. A. (1998) *Biochemistry 37*, 12431−12442.
76. Nishina, Y., Sato, K., Miura, R., Matsui, K., and Shiga, K. (1998) *J. Biochem. 124*, 200−208.
77. Czernuszewicz, R. S., Li, X.-Y., and Spiro, T. G. (1989) *J. Am. Chem. Soc. 111*, 7024−7031.
78. Ma, J.-G., Laberge, M., Song, X.-Z., Jentzen, W., Jia, S.-L., Zhang, J., Vanderkooi, J. M., and Shelnutt, J. A. (1998) *Biochemistry 37*, 5118−5128.
79. Kalsbeck, W. A., Ghosh, A., Pandey, R. K., Smith, K. M., and Bocian, D. F. (1995) *J. Am. Chem. Soc. 117*, 10959−10968.
80. Huang, Q., Laberge, M., Fidy, J., and Schweitzer-Stenner, R. (2002) in *Proceedings of XVIIIth International Conference on Raman Spectroscopy* (Mink, J., Jalsovszky, G., and Keresztury, G., Eds.) p 749, John Wiley & Sons, West Sussex.
81. Maltempo, M. M., Ohlsson, P. I., Paul, K. G., Petersson, L., and Ehrenberg, A. (1979) *Biochemistry 18*, 2935−2941.
82. Dasgupta, S., Rousseau, D. L., Anni, H., and Yonetani, T. (1989) *J. Biol. Chem. 264*, 654−662.
83. Smulevich, G., Feis, A., Focardi, C., Jeppe, T., and Welinder, G. (1994) *Biochemistry 33*, 15425−15432.

BI026992Y